

**Effects of quantum coherence and interference in atoms near nanoparticles**

Suman Dhayal and Yuri V. Rostovtsev

*Center for Nonlinear Sciences and Department of Physics, University of North Texas, 1155 Union Circle #311427, Denton, Texas 76203, USA*

(Received 27 January 2016; published 5 April 2016)

Optical properties of ensembles of realistic quantum emitters coupled to plasmonic systems are studied by using adequate models that can take into account full atomic geometry. In particular, the coherent effects such as forming “dark states,” optical pumping, coherent Raman scattering, and the stimulated Raman adiabatic passage (STIRAP) are revisited in the presence of metallic nanoparticles. It is shown that the dark states are still formed but they have more complicated structure, and the optical pumping and the STIRAP cannot be employed in the vicinity of plasmonic nanostructures. Also, there is a huge difference in the behavior of the local atomic polarization and the atomic polarization averaged over an ensemble of atoms homogeneously spread near nanoparticles. The average polarization is strictly related to the polarization induced by the external field, while the local polarization can be very different from the one induced by the external field. This is important for the excitation of single molecules, e.g., different components of scattering from single molecules can be used for their efficient detection.

DOI: [10.1103/PhysRevA.93.043405](https://doi.org/10.1103/PhysRevA.93.043405)**I. INTRODUCTION**

It is well known that metallic nanoparticles allow researchers to enhance electric fields via plasmonic interactions [1]. Although the enhancement of the field decreases very rapidly at even small distances from the nanoparticles, it is this enhanced field that is responsible for the many orders of magnitude enhancement of the Raman signal from molecules [2]. The plasmonic nanoparticles can be viewed as nanoantennas that are able to “focus” the field into relatively small regions that are much smaller than the wavelength of radiation. Optical (linear and nonlinear) and electronic properties of atoms and molecules experiencing huge field enhancement can be modified due to these plasmonic interactions. The plasmonic interaction also has a strong influence upon coherence effects.

The quantum coherence effects, such as coherent population trapping (CPT) [3] and electromagnetically induced transparency (EIT) [4–7], have been the focus of broad research activity for the last two decades, as they drastically change the optical properties of media. For example, for EIT in CW and pulsed regimes [5–9], absorption practically vanishes. The medium with excited quantum coherence, i.e., phaseonium [4], can be used to make an ultradispersive prism [10] that has several orders of magnitude higher angular spectral dispersion. The bending of light has also been demonstrated using the transverse dragging effect [11]. The corresponding steep dispersion results in the ultraslow (subluminal) or fast (superluminal) propagation of light pulses [12–16], which can produce huge optical delays [16] and can be used for drastic modification of the phase-matching conditions for Brillouin scattering [17], four-wave mixing [18], controllable switching between bunching and antibunching [19,20], storage and retrieval of pulses [21], freezing of a light pulse [22], and ultrahigh enhancement in absolute and relative rotation sensing using fast and slow light [23]. Recently, the coherent effects have been employed to theoretically demonstrate a quantum metamaterial with an all-optical and ultrafast (on the time scale inverse of the drive field Rabi frequency) control made of dense ultracold neutral atoms [24]. The so-called

hyperbolic metamaterials open a new realm of physics with exciting potential applications [25–28].

The quantum engineering of light-matter interaction at the nanoscale is an active field of research, and the quantum coherence and interference effects might have broad applications to novel nanoscale hybrid metal-semiconductor composites due to demonstrated field enhancement ranging from implementations of coherence effects [3–5] in nanostructures such as quantum dots and nanowires, and doped solids [29], to efficient radiators [30] and sensitive sensors, and efficient photovoltaics due to their unique structural, electrical, optical, and thermoelectric properties.

In this paper, we revisit the coherent effects in atomic and molecular systems located near nanoparticles. The first task here is to study the modification of the dark state of the atoms near the nanoparticles. The dark state, which is formed under the action of the coherent laser fields interacting with the atomic system, is the cornerstone of the coherent and quantum interference effects. Due to strong modification of the electromagnetic field near metallic as well as even near dielectric nanoparticles, the coherent population trapping state depends on the relative position of the atom with respect to the nanoparticle. The second task is to study the process of coherent control of the state of atoms via adiabatic change of the coherent laser field. The stimulated Raman adiabatic passage (STIRAP) [3–5] allows researchers to perform the adiabatic transformation of the “dark” states using the adiabatic change of the optical fields. We consider the STIRAP processes in atoms located near the dielectric or metallic nanoparticles. These processes are very efficient for creating maximal coherence in atomic and molecular media [30], and they are also important to control nanoparticles [31] and multilevel quantum systems [32]. The sensitivity of coherent Raman scattering can be improved by applying a femtosecond adaptive technique to excite maximal vibrational coherence to perform real-time identification of bacterial spores [33,34], and this technique has a potential to identify biomolecules as well. It was theoretically shown that chirped

laser pulses, even a single linearly chirped laser pulse, can be used for an efficient manipulation of the atomic population in ultracold Rb atoms [35–39]. Finally, the last task is to study the atomic responses' average over the position with respect to the nanoparticles.

## II. MODEL

We study the behavior of atoms in the presence of a field created by a nanoparticle. Because the electromagnetic fields are strongly changed by the presence of nanoparticles, we have to take into account the sufficient number of levels and develop a model that adequately describes the geometry of atomic states. For simplicity, we consider four- and seven-level atomic systems. In particular, to study the formation of the dark state, we consider the atomic transitions between a ground state  $F = 1$  and an excited state  $F' = 0$  (see Fig. 1). To perform simulations, we have to take into account all four atomic levels. The level structure under consideration can be found in alkali atoms, for example,  $^{87}\text{Rb}$ . The ground state  $5S_{1/2}$  consists of two hyperfine levels,  $F = 1$  and  $F = 2$ , and the excited state  $5P_{3/2}$  consists of four hyperfine levels,  $F' = 0$ ,  $F' = 1$ ,  $F' = 2$ , and  $F' = 3$ . Here we consider the transition between  $|F = 1, m\rangle$  and  $|F' = 0\rangle$ , which is a part of the  $D_2$  line. The Hamiltonian is given by

$$\hat{H}_{\text{total}} = \hat{H}_0 + \hat{V},$$

where  $\hat{H}_0$  is given by

$$H_0 = \mathcal{E}_1|1\rangle\langle 1| + \mathcal{E}_2|2\rangle\langle 2| + \mathcal{E}_3|3\rangle\langle 3| + \mathcal{E}_4|4\rangle\langle 4|,$$

and  $\mathcal{E}_1$ ,  $\mathcal{E}_2$ ,  $\mathcal{E}_3$ , and  $\mathcal{E}_4$  are the energies of the levels 1 ( $|F' = 0\rangle$ ), 2 ( $|F = 1, m = -1\rangle$ ), 3 ( $|F = 1, m = 0\rangle$ ), and 4 ( $|F = 1, m = +1\rangle$ ), respectively,  $\hat{V} = -\vec{\wp} \cdot \vec{E}$  describes the interaction of the atom with the electromagnetic field,  $\vec{\wp}$  is the operator of atomic dipole moment, and  $\vec{E}$  is the laser electric field. We consider that  $\vec{E}$  is the laser field modified by the nanoparticle that has all three components. Using the rotating-wave approximation (RWA), we can write the Hamiltonian as

$$\hat{H} = \hbar \begin{pmatrix} 0 & \Omega_1 & \Omega_2 & \Omega_3 \\ \Omega_1^* & \Delta_2 & 0 & 0 \\ \Omega_2^* & 0 & \Delta_3 & 0 \\ \Omega_3^* & 0 & 0 & \Delta_4 \end{pmatrix}, \quad (1)$$

where  $\Delta_2$ ,  $\Delta_3$ , and  $\Delta_4$  are the detunings of the frequencies  $\omega_2$ ,  $\omega_3$ , and  $\omega_4$  of the applied fields between levels 1 and

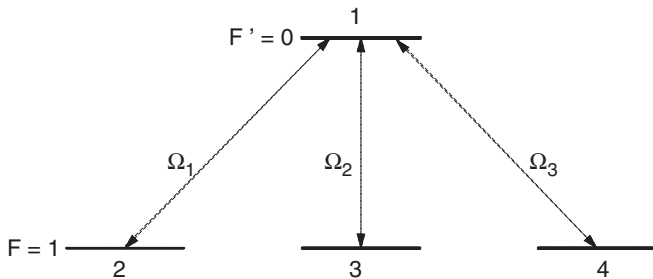


FIG. 1. The levels of a four-level atom.

2, 1 and 3, and 1 and 4, respectively, and  $\Omega_1$ ,  $\Omega_2$ ,  $\Omega_3$  are the Rabi frequencies,  $\Omega_\alpha = \wp_\alpha E_\alpha / \hbar$  (where  $\alpha$  denotes the corresponding transitions; see Fig. 1). The electric field and the dipole moment can be decomposed as  $\vec{E} = E_1 \hat{e}_- + E_2 \hat{z} + E_3 \hat{e}_+$  and  $\vec{\wp} = \wp_1 \hat{e}_- + \wp_2 \hat{z} + \wp_3 \hat{e}_+$ , where  $E_{1,3}$  are the amplitudes of the right and left circularly polarized electric fields,  $E_2$  is the amplitude of the linearly polarized electric field,

$$\wp_{1,3} = \langle F' = 0 | x \pm iy | F = 1, m = \pm 1 \rangle$$

and

$$\wp_2 = \langle F' = 0 | z | F = 1, m = 0 \rangle$$

are the matrix elements of the dipole moment,  $\hat{e}_\pm$  are the unit vectors of right and left circular polarizations, and  $\hat{z}$  is the unit vector of linear polarization.

We solve numerically the set of density matrix equations,

$$\dot{\rho} = -\frac{i}{\hbar} [\hat{H}, \rho] - \hat{\Gamma} \rho, \quad (2)$$

where  $\hat{\Gamma}$  is the matrix operator that describes the decay and relaxation processes in the system. The matrix operator  $\hat{\Gamma} \rho$  is given by

$$\hat{\Gamma} \rho = \begin{pmatrix} -\gamma_1 \rho_{11} & -\Gamma \rho_{12} & -\Gamma \rho_{13} & -\Gamma \rho_{14} \\ -\Gamma \rho_{21} & \gamma_2 \rho_{11} & -\gamma_0 \rho_{23} & -\gamma_0 \rho_{24} \\ -\Gamma \rho_{31} & -\gamma_0 \rho_{32} & \gamma_3 \rho_{11} & -\gamma_0 \rho_{34} \\ -\Gamma \rho_{41} & -\gamma_0 \rho_{42} & -\gamma_0 \rho_{43} & \gamma_4 \rho_{11} \end{pmatrix},$$

where  $\gamma_1$  is the relaxation rate of  $\rho_{11}$ ;  $\gamma_2$ ,  $\gamma_3$ , and  $\gamma_4$  are the relaxation rates of  $\rho_{11}$  to levels 2, 3, and 4, respectively;  $\Gamma$  is the relaxation rate of optical coherences, for example,  $\rho_{13}$ ,  $\rho_{12}$ , and  $\rho_{14}$ ; and  $\gamma_0$  is the relaxation rate of coherences between ground-state sublevels  $F = 1$ , for example,  $\rho_{23}$ ,  $\rho_{24}$ ,  $\rho_{34}$ . The relaxation rates are  $\gamma_1 = \gamma_2 + \gamma_3 + \gamma_4$ , and  $\Gamma = \gamma_{\text{col}} + (\gamma_1 + \gamma_0)/2$ , where  $\gamma_{\text{col}}$  is the relaxation due to collisions (for our simulations here, we use  $\gamma_{\text{col}} = 0$ ).

### A. Field distribution near nanoparticles

To find out the field distribution, we solve Maxwell's equations for fields  $\mathbf{E}$  and  $\mathbf{H}$ ,

$$\nabla \times \mathbf{H} = ikm^2 \mathbf{E}, \quad (3)$$

$$\nabla \times \mathbf{E} = -ik \mathbf{H}, \quad (4)$$

$$\nabla \cdot \mathbf{H} = 0, \quad (5)$$

$$\nabla \cdot \mathbf{E} = 0, \quad (6)$$

where  $k$  is the wave number, and  $m$  is the index of refraction of the medium. The fields satisfy the wave equations

$$\nabla^2 \mathbf{E} + k^2 m^2 \mathbf{E} = 0, \quad (7)$$

$$\nabla^2 \mathbf{H} + k^2 m^2 \mathbf{H} = 0. \quad (8)$$

Using the scalar potential  $\psi(r, \theta, \phi)$ , the wave equation

$$\nabla^2 \psi + k^2 m^2 \psi = 0 \quad (9)$$

has the solution that can be written as

$$\psi_{ln} = \begin{pmatrix} u \\ v \end{pmatrix} = \begin{pmatrix} \sin l\phi \\ \cos l\phi \end{pmatrix} P_n^l(\cos \theta) z_n(kr), \quad (10)$$

where  $P_n^l(\cos \theta)$  are the associated Legendre polynomials, and  $z_n(kr)$  are the spherical Bessel functions.

We introduce  $\mathbf{M}_\psi$  and  $\mathbf{N}_\psi$  for the fields (see, for example, [40]) as

$$\mathbf{M}_\psi = \nabla \times (\mathbf{r}\psi), \quad (11)$$

$$mk\mathbf{N}_\psi = \nabla \times \mathbf{M}_\psi, \quad (12)$$

which have the spherical components

$$M_r = 0, \quad kmN_r = \frac{\partial^2(r\psi)}{\partial r^2} + k^2 m^2 r\psi, \quad (13)$$

$$M_\theta = \frac{1}{r \sin \theta} \frac{\partial(r\psi)}{\partial \phi}, \quad kmN_\theta = \frac{1}{r} \frac{\partial^2(r\psi)}{\partial r \partial \theta}, \quad (14)$$

$$M_\phi = -\frac{1}{r} \frac{\partial(r\psi)}{\partial \theta}, \quad kmN_\phi = \frac{1}{r \sin \theta} \frac{\partial^2(r\psi)}{\partial r \partial \phi}. \quad (15)$$

Then, the fields  $\mathbf{E}$  and  $\mathbf{H}$  [solutions of Eq. (7) and Eq. (8)] can be written as

$$\mathbf{E} = \mathbf{M}_v + i\mathbf{N}_u, \quad (16)$$

$$\mathbf{H} = m(-\mathbf{M}_u + i\mathbf{N}_v). \quad (17)$$

We consider the case of a single sphere, and assume that the laser field is the plane wave (if the laser field is focused, that means that the focal spot is much larger than the wavelength of the laser beam), and the incident wave can be written as

$$\vec{E} = \vec{E}_0 e^{i\vec{k}\vec{r}}, \quad (18)$$

and potentials are given by

$$\psi = \begin{pmatrix} u \\ v \end{pmatrix} = \begin{pmatrix} \sin \phi \\ \cos \phi \end{pmatrix} \sum_{n=1}^{\infty} (-i)^n \frac{2n+1}{n(n+1)} P_n^1(\cos \theta) j_n(kr). \quad (19)$$

For the field scattered by the sphere, the potentials are

$$\begin{pmatrix} u \\ v \end{pmatrix} = \begin{pmatrix} \sin \phi \\ \cos \phi \end{pmatrix} \sum_{n=1}^{\infty} \begin{pmatrix} -a_n \\ -b_n \end{pmatrix} (-i)^n \frac{2n+1}{n(n+1)} P_n^1(\cos \theta) h_n^{(2)}(kr). \quad (20)$$

Inside the sphere, the potentials are given by

$$\begin{pmatrix} u \\ v \end{pmatrix} = \begin{pmatrix} \sin \phi \\ \cos \phi \end{pmatrix} \sum_{n=1}^{\infty} m \begin{pmatrix} c_n \\ d_n \end{pmatrix} (-i)^n \frac{2n+1}{n(n+1)} P_n^1(\cos \theta) j_n(kmr). \quad (21)$$

For the case of many spheres, the generalized Mie theory [41] can be used, where the approach is similar to [42,43] for layered media.

### B. Near-field approximation

Simple physics can be gained by considering the electric field close to spheres in a near-field dipole approximation (radius of the spheres is much smaller than the wavelength of

radiation,  $a \ll \lambda$ ). The electric field induced by polarization of the sphere is given by

$$E' = -\frac{4\pi}{3} P, \quad (22)$$

where the polarization is related to the field inside the sphere as

$$P = \frac{\epsilon - 1}{4\pi} E_{\text{in}}. \quad (23)$$

Then, the field inside the sphere is given by

$$E_{\text{in}} = E_0 + E' = \frac{3}{\epsilon + 2} E_0, \quad (24)$$

and polarization is

$$P = \frac{3}{4\pi} \frac{\epsilon - 1}{\epsilon + 2} E_0. \quad (25)$$

The corresponding dipole moment of the sphere related to the polarization as

$$p_i = Ql = \frac{4\pi}{3} R^3 P_i \quad (26)$$

can create an electric field that is given by

$$\vec{E}_p = \frac{3\hat{n}(\hat{n} \cdot \vec{p}) - \vec{p}}{r^3}. \quad (27)$$

Then, the field near the sphere is given by the external field and the field created by the dipole as

$$\vec{E} = \vec{E}_0 + \frac{\epsilon - 1}{\epsilon + 2} \frac{R^3}{r^3} [3\hat{n}(\hat{n} \cdot \hat{p}) - \hat{p}] E_0, \quad (28)$$

where  $\hat{n}$  and  $\hat{p}$  are corresponding unit vectors. One can see that at some frequencies where  $\epsilon + 2 \simeq 0$ , the electric field can be enhanced. For the case of many spheres, the dipoles induced in the sphere can be enhanced even more due to the dipole interaction between the gold nanoparticles. The rough estimation of the field enhancement based on this dipole approximation gives the same order of magnitude enhancement as that from the simulations based on the solution of the Maxwell's equations.

### III. MODIFICATION OF "DARK STATE"

The coherent effects can be described by using the so-called "dark" and "bright" states. Let us consider the fields at the resonance  $\Delta_2 = \Delta_3 = \Delta_4 = 0$ ; then the Hamiltonian given by Eq. (1) has the eigenvalues  $\pm\Omega_{\text{eff}} = \pm\sqrt{|\Omega_1|^2 + |\Omega_2|^2 + |\Omega_3|^2}$  corresponding to the bright states  $|B_{\pm}\rangle$  given by

$$|B_{\pm}\rangle = \frac{\pm\Omega_{\text{eff}}|1\rangle + \Omega_1|2\rangle + \Omega_2|3\rangle + \Omega_3|4\rangle}{\sqrt{2\Omega_{\text{eff}}^2}}, \quad (29)$$

and, for the zero eigenvalues, we have two dark states,

$$|D_1\rangle = \frac{-\Omega_2|2\rangle + \Omega_1|3\rangle}{\sqrt{|\Omega_1|^2 + |\Omega_2|^2}} \quad (30)$$

and

$$|D_2\rangle = \frac{-\Omega_3|2\rangle + \Omega_1|4\rangle}{\sqrt{|\Omega_1|^2 + |\Omega_3|^2}}. \quad (31)$$

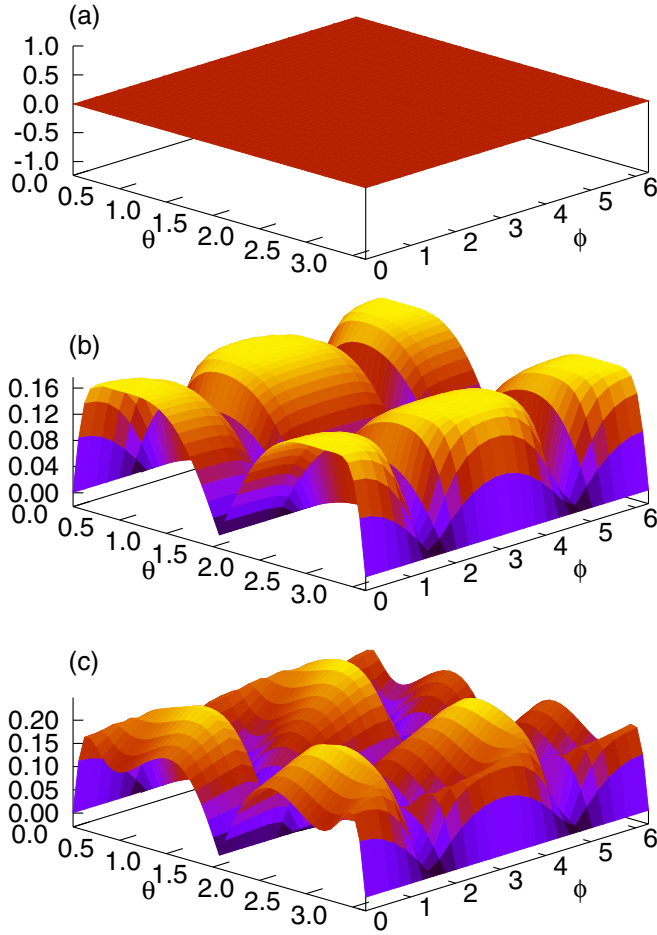


FIG. 2. Atomic coherence  $\rho_{23}$  (a) in vacuum, (b) in the vicinity of ZnO and (c) gold nanoparticles.

Then the atomic coherences  $\rho_{23}$  and  $\rho_{24}$  describe the dark states. We perform calculations of the atomic coherences  $\rho_{23}$  and  $\rho_{24}$  depending on the position of the atom near the sphere; the results are shown in Fig. 3.

Figure 2(a) depicts  $\rho_{23}$  in vacuum, and Figs. 2(b) and 2(c) represent it for ZnO and gold, respectively (we use the realistic parameters for gold from [44]). Figure 3(a) shows the plot of the absolute value of coherence  $\rho_{24}$  in vacuum, whereas Figs. 3(b) and 3(c) are those for ZnO and gold. The 3D dependence of absolute values of atomic coherence,  $\rho_{23}$ , are shown in Fig. 2(a). We can see that the dark states depend on the atomic position with respect to the nanoparticle.

#### IV. MODIFICATION OF STIRAP AND OPTICAL PUMPING

##### A. Stirap

Now we turn to the stimulated Raman adiabatic passage (STIRAP). The STIRAP allows researchers to perform the adiabatic transformation of the dark states using the adiabatic change of the optical fields [3–5]. To perform STIRAP, we assume that all of the atomic population is initially in the state 2, and we apply two short optical pulses  $E_1(t)$  and  $E_3(t)$  with left and right circular polarizations. The corresponding Rabi frequencies are

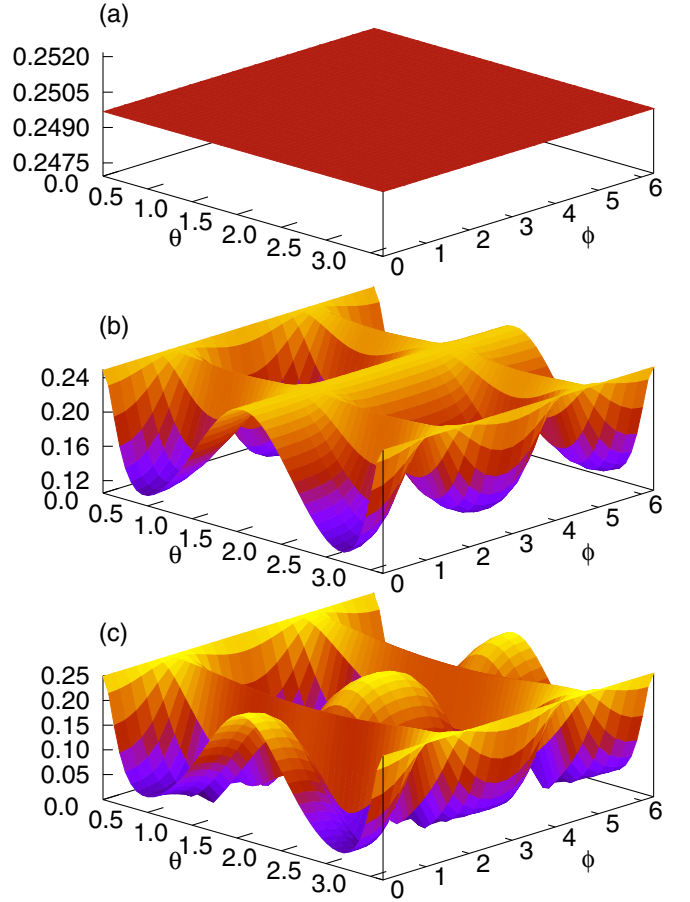


FIG. 3. Atomic coherence  $\rho_{24}$  (a) in vacuum, (b) in the vicinity of ZnO and (c) gold nanoparticles.

given by

$$\Omega_1 = \Omega_{01} \exp\left[-\frac{(t-t_1)^2}{2\tau^2}\right] \quad (32)$$

and

$$\Omega_3 = \Omega_{03} \exp\left[-\frac{(t-t_3)^2}{2\tau^2}\right], \quad (33)$$

where  $\Omega_{01}$  and  $\Omega_{03}$  are the amplitudes of the Rabi frequencies of optical pulses,  $\tau$  is the optical pulse width, and  $t_1$  and  $t_3$  are the time delays of STIRAP optical pulses (see Fig. 4). For simulations, we use  $\Omega_{01} = \Omega_{03} = 8\gamma_2$ ,  $\gamma_0 = 1 \cdot 10^{-3}\gamma_2$ ,  $\tau = 0.25\gamma_2^{-1}$ , and  $t_1 = 0.75\gamma_2^{-1}$  and  $t_3 = 1.25\gamma_2^{-1}$ .

Figures 5 and 6 show the time evolution of atomic populations,  $\rho_{22}$  and  $\rho_{44}$ , during the STIRAP. Figures 5(a)–5(c) depict the time evolution of the two populations in vacuum, in the presence of a dielectric sphere with dielectric constant,  $\epsilon = 1.55$ , and in the presence of a metallic nanoparticle with  $\epsilon = -2.1$ , respectively. We see from Figs. 5(a) and 5(b) that STIRAP works for materials with a small dielectric constant, but as the material deviates away from vacuum, it does not work. For example, Fig. 5(c) shows the time evolution of  $\rho_{22}$  and  $\rho_{44}$ , which is complicated.

In Fig. 6, we show the time evolution of atomic populations for the atom in the vicinity of a ZnO nanoparticle [Fig. 6(a)] and for a gold nanoparticle [Fig. 6(b)]. Again, we can see

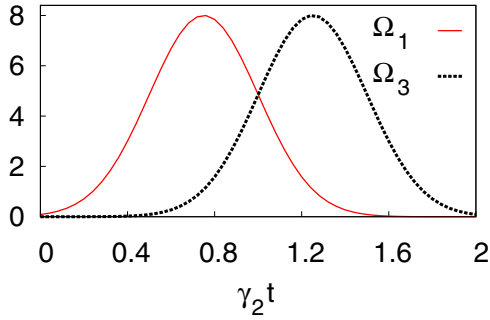


FIG. 4. Time evolution of the STIRAP pulses given by Eqs. (32) and (33).

from Figs. 6(a) and 6(b) that the atomic populations show a complicated distribution.

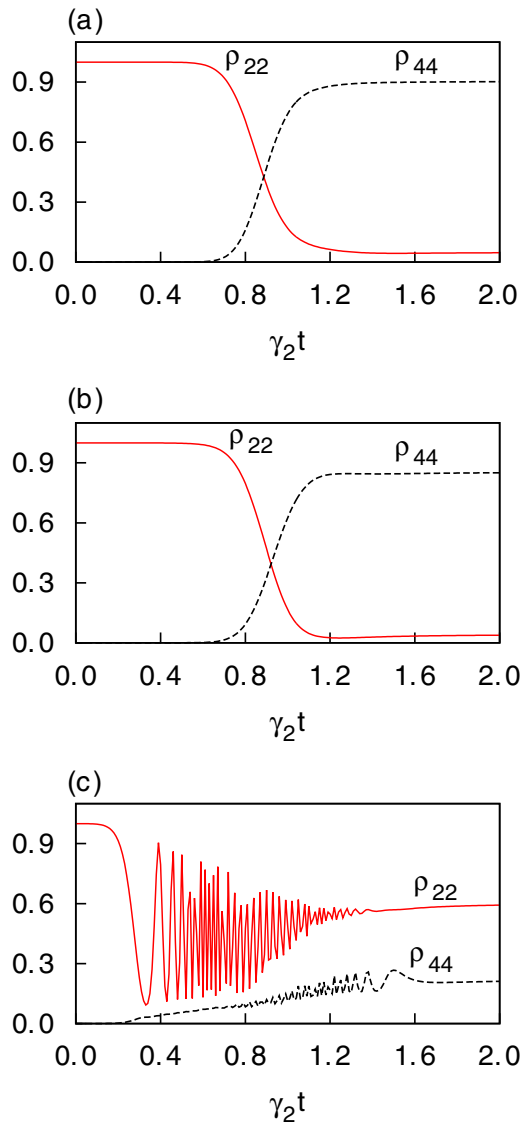


FIG. 5. Time evolution of atomic populations  $\rho_{22}$  and  $\rho_{44}$  during STIRAP (a) in vacuum, (b) in the presence of a dielectric sphere,  $\epsilon = 1.55$ , and (c) in the presence of a metallic nanoparticle,  $\epsilon = -2.1$ .

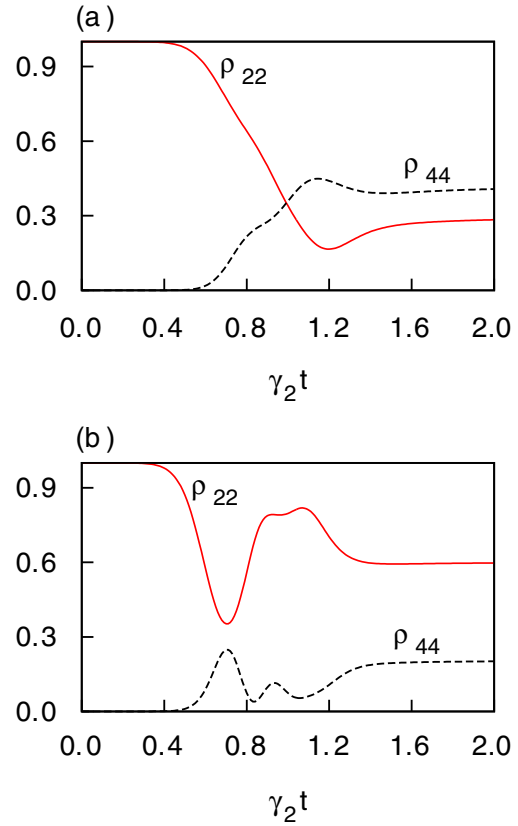


FIG. 6. Time evolution of atomic populations  $\rho_{22}$  and  $\rho_{44}$  during STIRAP (a) in the presence of a ZnO nanoparticle,  $\epsilon = 4.01$ , and (b) in the presence of a gold nanoparticle,  $\epsilon = -1.26 + i3.58$ .

### B. Optical pumping and STIRAP

In the previous section, we assume that all of the atomic population is initially in the state 2, but it is interesting to study whether it is possible to prepare the atom in this state. In vacuum, it is the optical pumping that can be used for this purpose. To simulate this process, we use a set of pulses to avoid coherent population trapping (as we have already seen in Sec. III, under the mutual action of fields  $\Omega_2$  and  $\Omega_3$ , the dark state is formed and some population is trapped in this state). We apply a pulse of the field  $\Omega_2$ , and then we apply a pulse of the field  $\Omega_3$ , namely, we apply the set of laser pulses to pump populations in levels 3 and 4 into level 2. The time evolution of the set of optical pumping pulses [consisting of  $E_1(t)$  and  $E_2(t)$ ] and the STIRAP optical pulses [consisting of  $E_1(t)$  and  $E_3(t)$ ] is shown in Fig. 7. At the end of the set of optical pumping pulses, two short optical left and right circularly polarized pulses  $E_1(t)$  and  $E_3(t)$  are applied, and the corresponding Rabi frequencies are given by

$$\begin{aligned} \Omega_1 = & \Omega_{01} \sin^2 \left( \frac{t}{T_m} \right) \exp \left[ -\frac{t^2}{2T_0^2} \right] \\ & + \Omega_{01} \exp \left[ -\frac{(t-t_1)^2}{2\tau^2} \right] \end{aligned} \quad (34)$$

and

$$\Omega_2 = \Omega_{02} \cos^2 \left( \frac{t}{T_m} \right) \exp \left[ -\frac{t^2}{2T_0^2} \right], \quad (35)$$

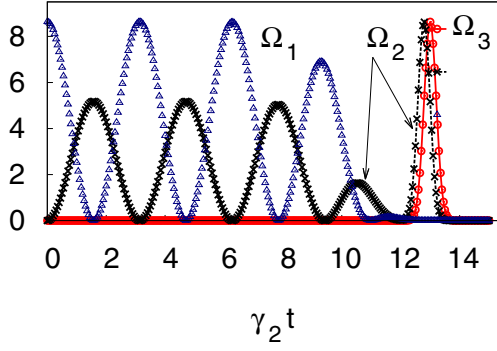


FIG. 7. Time evolution of the set of optical pumping and STIRAP pulses.

where  $\Omega_{02} = 5\gamma_2$  is the amplitude of the Rabi frequencies of a linearly polarized optical pulse,  $\Omega_{01} = 8\gamma_2$  and  $\Omega_{03} = 8\gamma_2$  [see Eqs. (32) and (33)] are the amplitudes of the Rabi frequencies of a circularly polarized optical pulse,  $\tau = 0.25\gamma_2^{-1}$ ,  $T_0 = 8\gamma_2^{-1}$  is the width of optical pumping,  $T_m = 1.5\gamma_2^{-1}$  is the modulation width of the optical pulses providing optical pumping, and  $t_1 = 12.25\gamma_2^{-1}$  and  $t_3 = 12.75\gamma_2^{-1}$  are the time delays of the STIRAP optical pulses.

We have also performed a simulation of the process of the optical pumping. Figure 8 shows the time dynamics of  $\rho_{22}$ ,  $\rho_{33}$ , and  $\rho_{44}$  during the pumping. Figures 8(a)–8(d) show the time dynamics in vacuum ( $\epsilon = 1.0$ ), in the presence of ZnO nanoparticle, in the presence of a metal nanoparticle with dielectric constant,  $\epsilon = -1.1$ , and in the presence of the gold nanoparticle.

## V. COHERENT RAMAN SCATTERING

In previous sections, we have demonstrated that dark states, optical pumping, and STIRAP in atoms near nanoparticles depend on the position of the atom with respect to the nanoparticle. In this section, we study the generation of optical fields by induced atomic coherence. This process is important to understand the coherent Raman scattering and its modification (such as, for example, enhancement) by nanoparticles [2].

In particular, we consider an atomic model that provides us with the correct description of all polarization components of the electromagnetic field near nanoparticles. The atomic level structure is shown in Fig. 9 with the Hamiltonian given by

$$H = \hbar \begin{pmatrix} 0 & \Omega_1 & \Omega_2 & \Omega_3 & \Omega_4 & \Omega_5 & \Omega_6 \\ \Omega_1^* & \Delta_2 & 0 & 0 & 0 & 0 & 0 \\ \Omega_2^* & 0 & \Delta_3 & 0 & 0 & 0 & 0 \\ \Omega_3^* & 0 & 0 & \Delta_4 & 0 & 0 & 0 \\ \Omega_4^* & 0 & 0 & 0 & \Delta_5 & 0 & 0 \\ \Omega_5^* & 0 & 0 & 0 & 0 & \Delta_6 & 0 \\ \Omega_6^* & 0 & 0 & 0 & 0 & 0 & \Delta_7 \end{pmatrix},$$

where  $\Delta_\alpha$  are the detunings from the atomic transitions (see Fig. 9),  $\Omega_1, \Omega_2, \Omega_3$  are the Rabi frequencies,  $\Omega_\alpha = \wp_\alpha E_\alpha^{(1)}/\hbar$  (where  $\alpha = 1, 2, 3$  denotes the corresponding transitions; see Fig. 9), and  $\Omega_4, \Omega_5, \Omega_6$  are the Rabi frequencies,  $\Omega_\alpha =$

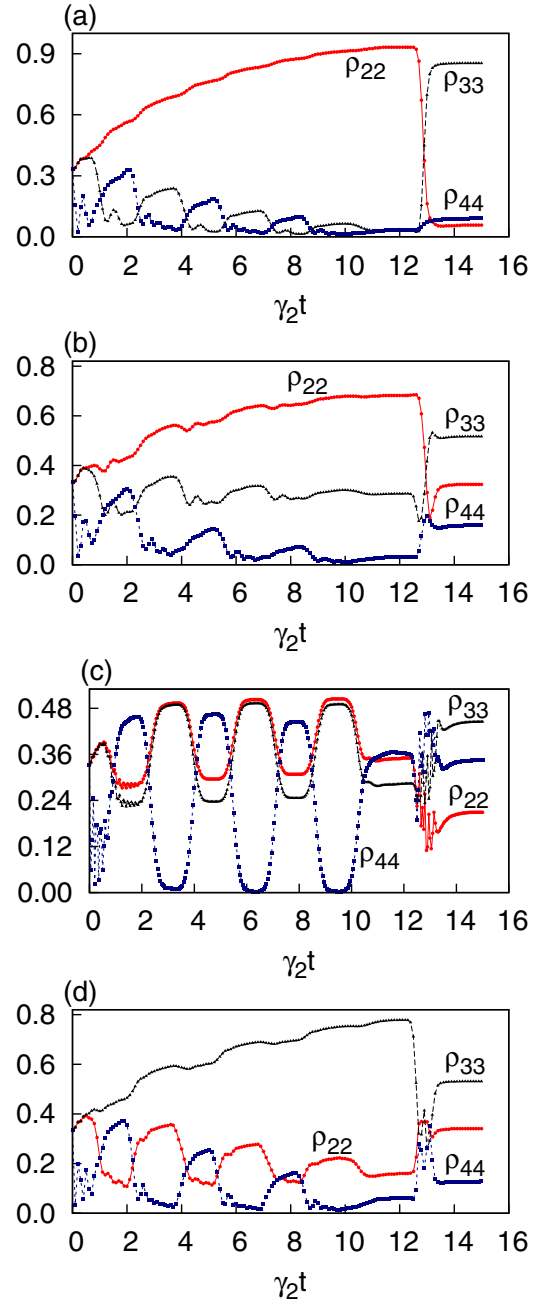


FIG. 8. Time dynamics of atomic populations  $\rho_{22}$ ,  $\rho_{33}$ , and  $\rho_{44}$  during optical pumping (a) in vacuum, (b) in the presence of a ZnO nanoparticle, (c) in the presence of a metal nanoparticle with dielectric constant,  $\epsilon = -1.1$ , and (d) in the presence of a gold nanoparticle.

$\tilde{\wp}_\alpha E_\alpha^{(2)}/\hbar$  (where  $\alpha = 4, 5, 6$  denotes the corresponding transitions; see Fig. 9).

The electric field  $\vec{E}^{(1)}$  is close to the resonance to transitions  $F' = 0$  and  $F = 1$ , and the electric field  $\vec{E}^{(2)}$  is close to the resonance to transitions  $F' = 0$  and  $F = 1'$ , and the fields can be decomposed as  $\vec{E}^{(1)} = E_1^{(1)}\hat{e}_- + E_2^{(1)}\hat{z} + E_3^{(1)}\hat{e}_+$  and  $\vec{E}^{(2)} = E_1^{(2)}\hat{e}_- + E_2^{(2)}\hat{z} + E_3^{(2)}\hat{e}_+$ . The dipole moments of corresponding transitions can be decomposed as  $\vec{\wp} = \wp_1\hat{e}_- +$

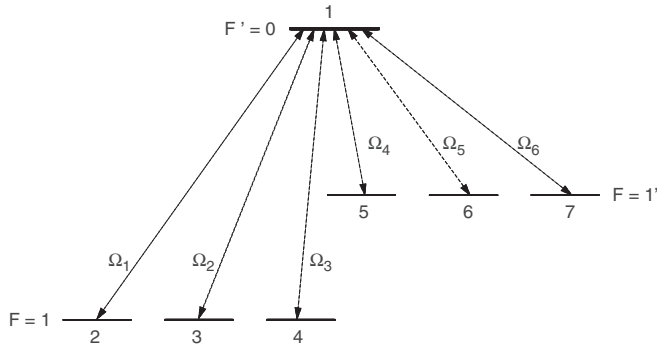


FIG. 9. The levels of a seven-level atom.

$\wp_{2\hat{z}} + \wp_{3\hat{e}_+}$  and  $\vec{\wp} = \wp_1\hat{e}_- + \wp_2\hat{z} + \wp_3\hat{e}_+$ , where

$$\wp_{1,3} = \langle F' = 0 | x \pm iy | F = 1, m = \pm 1 \rangle,$$

$$\wp_2 = \langle F' = 0 | z | F = 1, m = 0 \rangle,$$

$$\wp_{4,6} = \langle F' = 0 | x \pm iy | F = 1', m = \pm 1 \rangle,$$

$$\wp_5 = \langle F' = 0 | z | F = 1', m = 0 \rangle$$

are the matrix elements of the dipole moment.

We consider that the circularly polarized and resonant to transitions laser pulses induce the atomic coherence at the low-frequency transition between sublevels of  $F = 1$  and  $F = 1'$  (see Fig. 9). Then, at a later time, the circularly polarized laser pulse at the transition is applied to the atomic system and it induces a pulse of the atomic polarization that generates a coherent Raman optical pulse (see the time evolution of the pulses for coherent Raman scattering in Fig. 10). The corresponding Rabi frequencies are given by

$$\Omega_1 = \Omega_{01} \exp\left[-\frac{(t-t_1)^2}{2\tau^2}\right] + \Omega_{012} \exp\left[-\frac{(t-t_{12})^2}{2\tau^2}\right] \text{ and}$$

$$\Omega_4 = \Omega_{04} \exp\left[-\frac{(t-t_4)^2}{2\tau^2}\right], \quad (36)$$

where  $\Omega_{01}$ ,  $\Omega_{012}$ , and  $\Omega_{04}$  are the amplitudes of the Rabi frequencies of optical pulses,  $\tau$  is the optical pulse width, and  $t_1$ ,  $t_{12}$ , and  $t_4$  are the time delays (see Fig. 4). For simulations, we

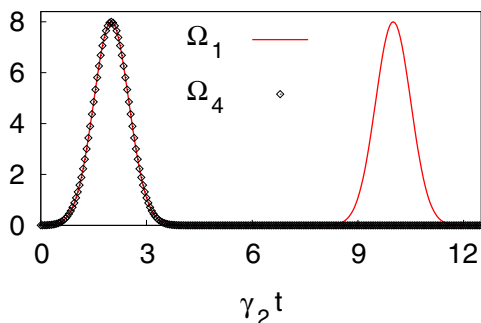
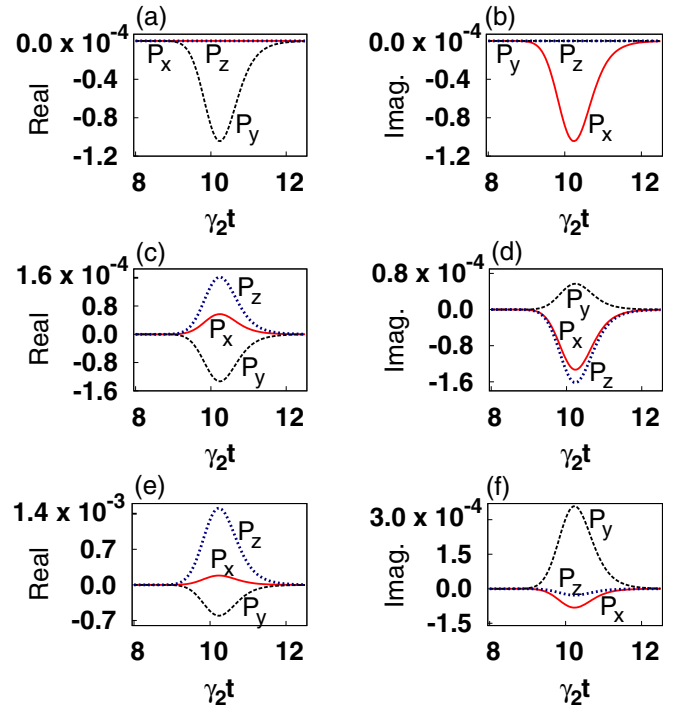
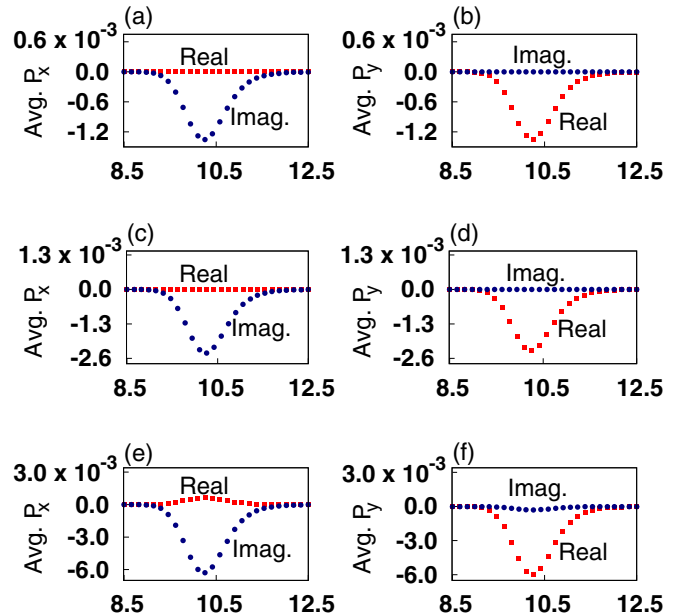


FIG. 10. Time evolution of the pulses for coherent Raman scattering given by Eq. (36).

FIG. 11. Real and imaginary parts of polarization components for the incident field amplitude,  $\Omega_{04} = 0.1\gamma_2$ . (a),(b) Real and imaginary components in vacuum, (c),(d) real and imaginary components in the presence of a ZnO nanoparticle, and (e),(f) real and imaginary components in the presence of a gold nanoparticle.FIG. 12. Average polarizations  $P_x$  and  $P_y$  for  $\Omega_{04} = 0.1\gamma_2$ . (a),(c),(e) Real and imaginary components of polarization  $P_x$  along the x axis in vacuum, in the presence of ZnO and gold nanoparticles, respectively. Similarly, (b),(d),(f) real and imaginary components of polarization  $P_x$  along the y axis in vacuum, in the presence of ZnO and gold nanoparticles, respectively.

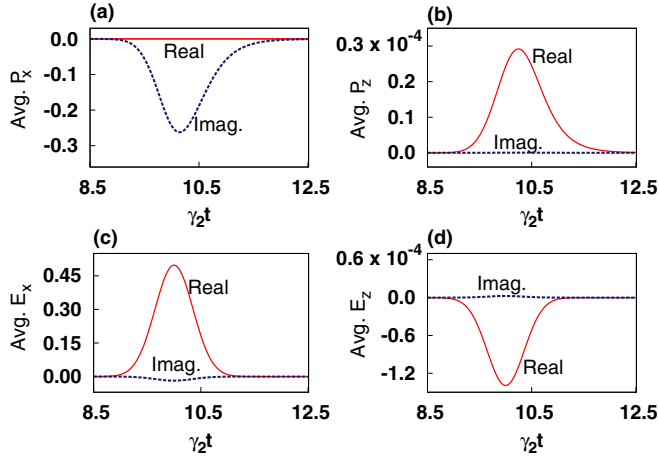


FIG. 13. Average polarization components  $P_x$  and  $P_z$ , and average field components  $E_x$  and  $E_z$  over the sphere using the Mie field for a ZnO nanoparticle of 2 nm radius. (a) Real and imaginary parts of average polarization  $P_x$ , (b) real and imaginary parts of average polarization  $P_z$ ; (c) and (d) correspond to  $E_x$  and  $E_z$ .

use  $\Omega_{01} = \Omega_{012} = \Omega_{04} = 8\gamma_2$ ,  $\gamma_0 = 1 \cdot 10^{-3}\gamma_2$ ,  $\tau = 0.5\gamma_2^{-1}$ ,  $t_1 = t_4 = 1.5\gamma_2^{-1}$ , and  $t_{12} = 10.5\gamma_2^{-1}$ .

Figure 11 shows time variations of induced polarization components  $P_x$ ,  $P_y$ , and  $P_z$  over time for different nanoparticles at incident field amplitudes,  $\Omega_{04} = 0.1\gamma_2$ . Figures 11(a), 11(c), and 11(e) show the variations of real components of  $P_x$ ,  $P_y$ , and  $P_z$  in vacuum for a ZnO nanoparticle and for a gold nanoparticle, respectively. Similarly, Figs. 11(b), 11(d), and 11(f) represent the imaginary parts of  $P_x$ ,  $P_y$ , and  $P_z$  for the same material nanoparticles, respectively. We have also observed that as the incident field amplitude increases, there is a dependence in the variation of polarization components, but it is not significant.

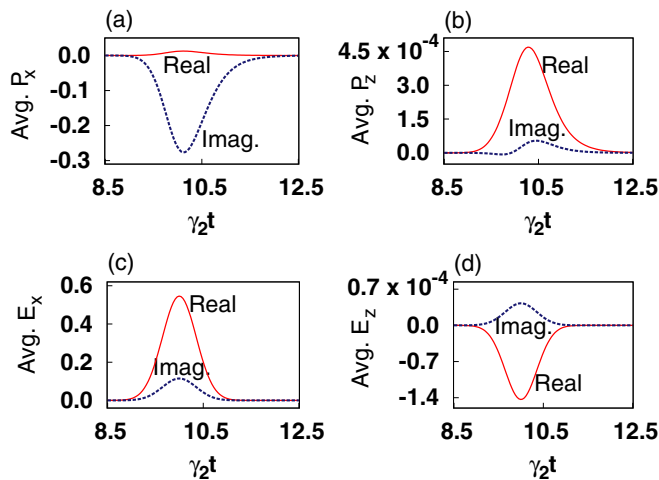


FIG. 14. Average polarization components  $P_x$  and  $P_z$ , and average field components  $E_x$  and  $E_z$  over the sphere using the Mie field for a ZnO nanoparticle of 40 nm radius. (a) Real and imaginary parts of average polarization  $P_x$ , (b) real and imaginary parts of average polarization  $P_z$ ; (c) and (d) correspond to  $E_x$  and  $E_z$ .

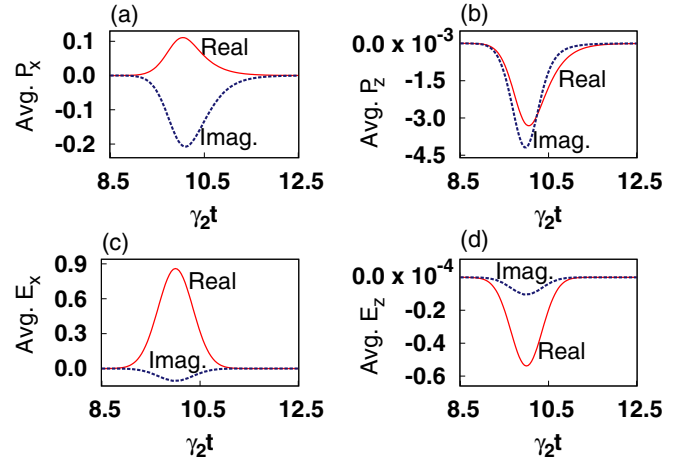


FIG. 15. Average polarization components  $P_x$  and  $P_z$ , and average field components  $E_x$  and  $E_z$  over the sphere using the Mie field for a ZnO nanoparticle of 100 nm radius. (a) Real and imaginary parts of average polarization  $P_x$ , (b) real and imaginary parts of average polarization  $P_z$ ; (c) and (d) correspond to  $E_x$  and  $E_z$ .

#### A. Average of atomic response and average field

We can see that the atomic response depends on the position with respect to the nanoparticle. The field created by the nanoparticle modifies the external field. In this regard, a question arises regarding how the average atomic response over the position of the atom is with respect to the field.

The average field can be easily found for the near field of the nanoparticle that is much smaller than the wavelength,  $a \ll \lambda$ . Indeed, according to the near field given by Eq. (28),

$$\langle E \rangle = E_0 - \frac{\epsilon - 1}{\epsilon + 2} E_0 = \frac{3}{\epsilon + 2} E_0. \quad (37)$$

The averaging above is defined as

$$\langle Q \rangle \equiv \frac{1}{4\pi} \int_0^{2\pi} \int_0^\pi Q(\theta, \phi) \sin \theta \, d\theta \, d\phi. \quad (38)$$

For ZnO nanoparticles,  $\epsilon \simeq 4$ , the average field  $\langle E \rangle \simeq 0.5E_0$ .

Then we calculate the average polarizations over the spheres. Figures 12 show the time variation of the average polarizations for the same incident fields as those for the polarization components. Figures 12(a), 12(c), and 12(e) represent real and imaginary components of polarization  $P_x$  along the  $x$  axis in vacuum, in the presence of ZnO and gold nanoparticles, respectively, and Figs. 12(b), 12(d), and 12(f) represent those of polarization  $P_y$  along the  $y$  axis in vacuum, in the presence of ZnO and gold nanoparticles, respectively.

Figures 13–16 show the average polarization components  $P_x$  and  $P_z$ , and the average field components  $E_x$  and  $E_z$  over the sphere using the Mie field for a ZnO nanoparticle of radii 2, 40, 100, and 400 nm, respectively. Figures 13(a) and 13(b) through Figs. 16(a) and 16(b) represent the real and imaginary parts of average polarization components  $P_x$  and  $P_z$ , respectively, and Figs. 13(c) and 13(d) through Figs. 16(c) and 16(d) correspond to the real and imaginary parts of average fields components  $E_x$  and  $E_z$  over the spheres, respectively.

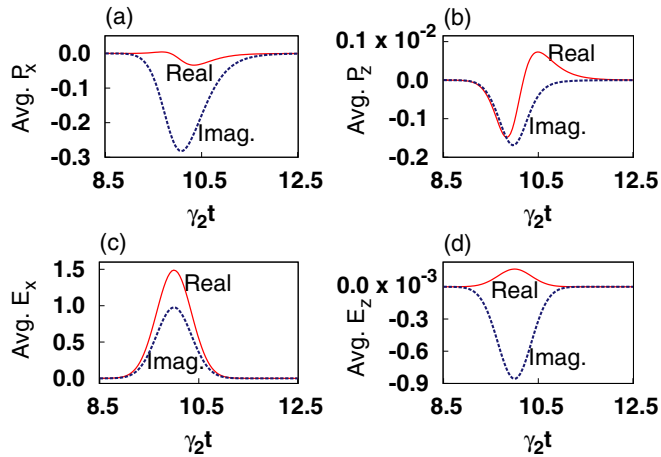


FIG. 16. Average polarization components  $P_x$  and  $P_z$ , and average field components  $E_x$  and  $E_z$  over the sphere using the Mie field for a ZnO nanoparticle of 400 nm radius. (a) Real and imaginary parts of average polarization  $P_x$ , (b) real and imaginary parts of average polarization  $P_z$ ; (c) and (d) correspond to  $E_x$  and  $E_z$ .

## VI. CONCLUSION

In conclusion, we have demonstrated that the optical properties of atoms and molecules coupled to plasmonic systems are strongly modified and changed. We develop and use accordingly the adequate atomic models, properly taking into account atomic geometry. We have shown that, indeed, the structure of dark states depends on the location of the atom with respect to the nanoparticle and the three-level models cannot be properly used to describe the interaction of radiation with the atomic systems. We demonstrate the formation of dark states, optical pumping, coherent Raman scattering, and the stimulated Raman adiabatic passage (STIRAP) in the presence

of metallic nanoparticles. It is shown that the dark states are still formed but they have more complicated structure, and the optical pumping and the STIRAP cannot be employed in the vicinity of plasmonic nanostructures. The STIRAP technique should be carefully used because it might not work or at least has new features in the presence of nanoparticles. Also there is a huge difference between the local atomic polarization and the atomic polarization averaged over an ensemble of atoms homogeneously spread near nanoparticles. The averaged polarization is strictly related to the polarization of the external field, while the local polarization can be very different from the one induced by the external field. This is important for the excitation of single molecules, e.g., different components of scattering from single molecules can be used for efficient detection of nanoparticles. These features mentioned above are important because they may lead to new applications such as the appearance of vortices of radiation near the nanoparticles that can demonstrate the rotational Doppler effect. Thus an extremely compact sensor of rotation can be developed on the basis of these effects. Note that these effects open a way to detect rotations which is different from Sagnac interferometry [45–48]. Let us stress here that the demonstrated implementations of coherence effects in nanostructures and nanoparticles have broad applications to doped solids [29] to develop efficient radiators and sensitive sensors, and efficient photovoltaics due to their unique structural, electrical, and optical properties.

## ACKNOWLEDGMENTS

We thank Vladimir Drachev, Norbert Kroo, and Susanne Yelin for helpful and fruitful discussions. S.D. and Y.R. gratefully acknowledge the support from the UNT Research Initiation Grant and the summer fellowship UNT program.

- 
- [1] M. I. Stockman, Nanoplasmonics: past, present, and glimpse into future, *Opt. Express* **19**, 22029 (2011).
- [2] M. Moskovits, Surface-enhanced Raman spectroscopy: A brief perspective, in *Surface-Enhanced Raman Scattering Physics and Applications* (Springer-Verlag, Berlin, Heidelberg, 2006), pp. 1–18.
- [3] E. Arimondo, in *Progress in Optics*, edited by E. Wolf (Elsevier Science, Amsterdam, 1996), Vol. XXXV, p. 257.
- [4] M. O. Scully and M. S. Zubairy, *Quantum Optics* (Cambridge University Press, Cambridge, 1997).
- [5] S. E. Harris, Electromagnetically induced transparency, *Phys. Today* **50**(7), 36 (1997).
- [6] S. E. Harris, Electromagnetically Induced Transparency with Matched Pulses, *Phys. Rev. Lett.* **70**, 552 (1993).
- [7] M. Fleischhauer, A. Imamoglu, and J. P. Marangos, Electromagnetically induced transparency: Optics in coherent media, *Rev. Mod. Phys.* **77**, 633 (2005).
- [8] O. Kocharovskaya and Ya. I. Khanin, Population trapping and coherent bleaching of a three-level medium by a periodic train of ultrashort pulses, *Sov. Phys. JETP* **63**, 945 (1986).
- [9] V. A. Sautenkov, Y. V. Rostovtsev, C. Y. Ye, G. R. Welch, O. Kocharovskaya, and M. O. Scully, Electromagnetically induced transparency in rubidium vapor prepared by a comb of short optical pulses, *Phys. Rev. A* **71**, 063804 (2005).
- [10] V. A. Sautenkov, H. Li, Y. V. Rostovtsev, and M. O. Scully, Ultradispersive adaptive prism based on a coherently prepared atomic medium, *Phys. Rev. A* **81**, 063824 (2010).
- [11] I. Carusotto, M. Artoni, G. C. La Rocca, and F. Bassani, Transverse Fresnel-Fizeau drag effects in strongly dispersive media, *Phys. Rev. A* **68**, 063819 (2003).
- [12] L. V. Hau, S. E. Harris, Z. Dutton, and C. H. Behroozi, Light speed reduction to 17 metres per second in an ultracold atomic gas, *Nature (London)* **397**, 594 (1999); C. Liu, Z. Dutton, C. H. Behroozi, and L. V. Hau, Observation of coherent optical information storage in an atomic medium using halted light pulses, *ibid.* **409**, 490 (2001).
- [13] M. M. Kash, V. A. Sautenkov, A. S. Zibrov, L. Hollberg, G. R. Welch, M. D. Lukin, Y. Rostovtsev, E. S. Fry, and M. O. Scully, Ultraslow Group Velocity and Enhanced Nonlinear Optical Effects in a Coherently Driven Hot Atomic Gas, *Phys. Rev. Lett.* **82**, 5229 (1999); D. Budker, D. F. Kimball, S. M. Rochester, and V. V. Yashchuk, Nonlinear Magneto-optics and Reduced Group Velocity of Light in Atomic Vapor with Slow Ground State Relaxation, *ibid.* **83**, 1767 (1999).

- [14] L. J. Wang, A. Kuzmich, and A. Dogariu, Gain-assisted superluminal light propagation, *Nature (London)* **406**, 277 (2000); A. Dogariu, A. Kuzmich, and L. J. Wang, Transparent anomalous dispersion and superluminal light-pulse propagation at a negative group velocity, *Phys. Rev. A* **63**, 053806 (2001).
- [15] G. S. Agarwal, T. N. Dey, and S. Menon, Knob for changing light propagation from subluminal to superluminal, *Phys. Rev. A* **64**, 053809 (2001).
- [16] E. E. Mikhailov, V. A. Sautenkov, Y. V. Rostovtsev, and G. R. Welch, Absorption resonance and large negative delay in rubidium vapor with a buffer gas, *J. Opt. Soc. Am. B* **21**, 425 (2004); Q. Sun, Y. V. Rostovtsev, J. P. Dowling, M. O. Scully, and M. S. Zubairy, Optically controlled delays for broadband pulses, *Phys. Rev. A* **72**, 031802 (2005).
- [17] A. B. Matsko, Y. V. Rostovtsev, M. Fleischhauer, and M. O. Scully, Anomalous Stimulated Brillouin Scattering via Ultraslow Light, *Phys. Rev. Lett.* **86**, 2006 (2001).
- [18] Y. V. Rostovtsev, Z.-E. Sariyanni, and M. O. Scully, Electromagnetically Induced Coherent Backscattering, *Phys. Rev. Lett.* **97**, 113001 (2006).
- [19] V. A. Sautenkov, Y. V. Rostovtsev, and M. O. Scully, Switching between photon-photon correlations and Raman anticorrelations in a coherently prepared Rb vapor, *Phys. Rev. A* **72**, 065801 (2005).
- [20] M. Fleischhauer and M. D. Lukin, Dark-State Polaritons in Electromagnetically Induced Transparency, *Phys. Rev. Lett.* **84**, 5094 (2000); Quantum memory for photons: Dark-state polaritons, *Phys. Rev. A* **65**, 022314 (2002); D. F. Phillips, A. Fleischhauer, A. Mair, R. L. Walsworth, and M. D. Lukin, Storage of Light in Atomic Vapor, *Phys. Rev. Lett.* **86**, 783 (2001).
- [21] A. B. Matsko, Y. V. Rostovtsev, O. Kocharovskaya, A. S. Zibrov, and M. O. Scully, Nonadiabatic approach to quantum optical information storage, *Phys. Rev. A* **64**, 043809 (2001); C. Mewes and M. Fleischhauer, Two-photon linewidth of light “stopping” via electromagnetically induced transparency, *ibid.* **66**, 033820 (2002); T. N. Dey and G. S. Agarwal, Storage and retrieval of light pulses at moderate powers, *ibid.* **67**, 033813 (2003).
- [22] O. Kocharovskaya, Y. Rostovtsev, and M. O. Scully, Stopping Light via Hot Atoms, *Phys. Rev. Lett.* **86**, 628 (2001).
- [23] M. S. Shahriar, G. S. Pati, R. Tripathi, V. Gopal, M. Messall, and K. Salit, Ultrahigh enhancement in absolute and relative rotation sensing using fast and slow light, *Phys. Rev. A* **75**, 053807 (2007).
- [24] P. K. Jha, M. Mrejen, J. Kim, C. Wu, Y. Wang, Y. V. Rostovtsev, and X. Zhang, Coherence-Driven Topological Transition in Quantum Metamaterials, *Phys. Rev. Lett.* (to be published).
- [25] V. Shalaev, Optical negative-index metamaterials, *Nat. Photon.* **1**, 41 (2007).
- [26] Y. Liu and X. Zhang, Metamaterials: a new frontier of science and technology, *Chem. Soc. Rev.* **40**, 2494 (2011).
- [27] N. I. Zheludev and Y. S. Kivshar, From metamaterials to metadevices, *Nat. Mater.* **11**, 917 (2012).
- [28] A. Poddubny, I. Iprsh, P. Belov, and Y. Kivshar, Hyperbolic metamaterials, *Nat. Photon.* **7**, 948 (2013).
- [29] N. G. Kalugin and Y. V. Rostovtsev, “Dark” and “bright” excitons in carbon nanotubes: New media for quantum optics, *J. Nanoelectron. Optoelectron.* **4**, 302 (2009).
- [30] N. G. Kalugin and Y. V. Rostovtsev, Efficient generation of short terahertz pulses via stimulated Raman adiabatic passage, *Opt. Lett.* **31**, 969 (2006).
- [31] M. Sukharev and S. A. Malinovskaya, Stimulated Raman adiabatic passage as a route to achieving optical control in plasmonics, *Phys. Rev. A* **86**, 043406 (2012).
- [32] P. Kumar, S. A. Malinovskaya, and V. S. Malinovsky, Optimal control of multilevel quantum systems in the field-interaction representation, *Phys. Rev. A* **90**, 033427 (2014).
- [33] M. O. Scully, G. W. Kattawar, B. P. Lucht, T. Opatrny, H. Pilloff, A. Rebane, A. V. Sokolov, and M. S. Zubairy, FAST CARS: Engineering a laser spectroscopic technique for rapid identification of bacterial spores, *Proc. Natl. Acad. Sci. USA* **99**, 10994 (2002).
- [34] D. Pestov, R. K. Murawski, G. O. Ariunbold, X. Wang, M. Zhi, A. V. Sokolov, V. A. Sautenkov, Y. V. Rostovtsev, A. Dogariu, Y. Huang, and M. O. Scully, Optimizing the laser pulse configuration for coherent Raman spectroscopy, *Science* **316**, 265 (2007).
- [35] T. A. Collins and S. A. Malinovskaya, Manipulation of ultracold Rb atoms using a single linearly chirped laser pulse, *Opt. Lett.* **37**, 2298 (2012).
- [36] S. A. Malinovskaya, Prevention of decoherence by two femtosecond chirped pulse trains, *Opt. Lett.* **33**, 2245 (2008).
- [37] S. A. DeSavage, J. P. Davis, and F. A. Narducci, Controlling Raman resonances with magnetic fields, *J. Mod. Opt.* **60**, 95 (2013).
- [38] D. Sun, Z.-E. Sariyanni, S. Das, and Y. V. Rostovtsev, Propagation of  $0\pi$  pulses in a gas of three-level atoms, *Phys. Rev. A* **83**, 063815 (2011).
- [39] Z.-E. Sariyanni, D. Sun, and Y. V. Rostovtsev, Stimulated Raman spectroscopy with  $0\pi$  pulses, *Opt. Lett.* **39**, 766 (2014).
- [40] H. C. van de Hulst, *Light Scattering by Small Particles* (Dover, New York, 1981).
- [41] S. Dhayal, G. Sapkota, U. Philipose, and Y. Rostovtsev, Photovoltaics based on nanotubes filled with nanoparticles: generalized Mie theory approach, *J. Mod. Opt.* **60**, 73 (2013).
- [42] P. Yeh, *Optical Waves in Layered Media*, Wiley Series in Pure and Applied Optics (Wiley, New York, 1988).
- [43] M. Schubert, Polarization-dependent optical parameters of arbitrarily anisotropic homogeneous layered systems, *Phys. Rev. B* **53**, 4265 (1996).
- [44] P. G. Etchegoin, E. C. Le Ru, and M. Meyer, An analytic model for the optical properties of gold, *J. Chem. Phys.* **125**, 164705 (2006); Erratum: “An analytic model for the optical properties of gold” [*J. Chem. Phys.* **125**, 164705 (2006)], **127**, 189901 (2007).
- [45] M. G. Sagnac, L’*éther lumineux démontré parl’ effet du vent relatif d’*éther* dans un interféromètre en rotation uniforme*, C. R. Acad. Sci. **157**, 708 (1913).
- [46] E. J. Post, Sagnac effect, *Rev. Mod. Phys.* **39**, 475 (1967).
- [47] G. B. Malykin, The Sagnac effect: correct and incorrect explanations, *Phys. Usp.* **43**, 1229 (2000).
- [48] P. G. Eleseev, Theory of nonlinear Sagnac effect, *Opto-Electron. Rev.* **16**, 118 (2008).